Contactless electrical conductivity measurement of metallic submicron-grain material: Application to the study of aluminum with severe plastic deformation

M. Mito, H. Matsui, T. Yoshida, T. Anami, K. Tsuruta, H. Deguchi, T. Iwamoto, D. Terada, Y. Miyajima, and N. Tsuji

---

Articles you may be interested in

Noncontact evaluation of the dependency of electrical conductivity on stress for various Al alloys as a function of plastic deformation and annealing
J. Appl. Phys. **108**, 024909 (2010); 10.1063/1.3456996

Measurement of electrical conductivity in nonferromagnetic tubes and rods at low frequencies
Am. J. Phys. **77**, 949 (2009); 10.1119/1.3184154

Vacancy clusters in ultrafine grained Al by severe plastic deformation
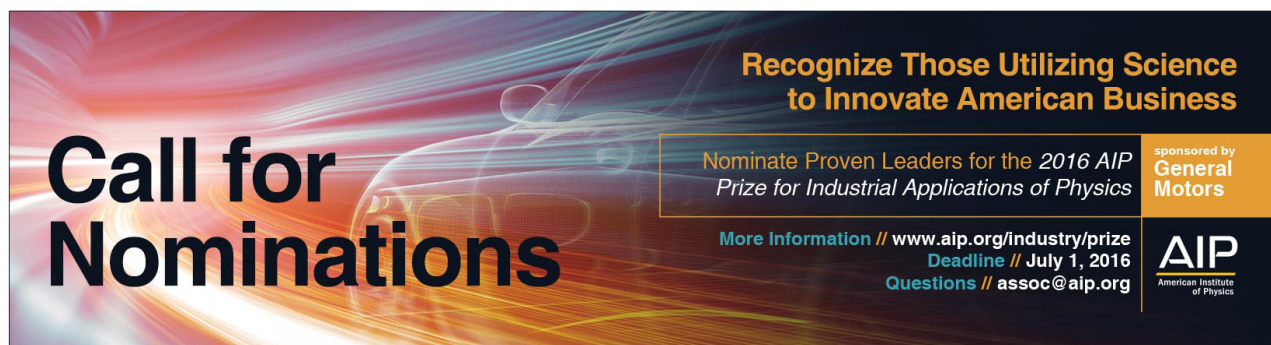Appl. Phys. Lett. **91**, 141908 (2007); 10.1063/1.2794416

Nucleation of deformation twins in nanocrystalline face-centered-cubic metals processed by severe plastic deformation
J. Appl. Phys. **98**, 034319 (2005); 10.1063/1.2006974

Magnetization curves of plastically deformed Fe metals and alloys
J. Appl. Phys. **87**, 805 (2000); 10.1063/1.371945

Contactless electrical conductivity measurement of metallic submicron-grain material: Application to the study of aluminum with severe plastic deformation

M. Mito,[1,a)] H. Matsui,[1] T. Yoshida,[1] T. Anami,[1] K. Tsuruta,[1] H. Deguchi,[1] T. Iwamoto,[2] D. Terada,[3] Y. Miyajima,[4] and N. Tsuji[5]

[1]*Graduate School of Engineering, Kyushu Institute of Technology, Kitakyushu 804-8550, Japan*
[2]*Institute for Materials Chemistry and Engineering, Kyushu University, Fukuoka 819-0395, Japan*
[3]*Faculty of Engineering, Chiba Institute of Technology, Narashino 275-0016, Japan*
[4]*School of Materials and Chemical Technology, Tokyo Institute of Technology, Yokohama 226-8502, Japan*
[5]*Graduate School of Engineering, Kyoto University, Kyoto 606-8501, Japan*

We measured the electrical conductivity σ of aluminum specimen consisting of submicron-grains by observing the AC magnetic susceptibility resulting from the eddy current. By using a commercial platform for magnetic measurement, contactless measurement of the relative electrical conductivity σ_n of a nonmagnetic metal is possible over a wide temperature (T) range. By referring to σ at room temperature, obtained by the four-terminal method, $\sigma_n(T)$ was transformed into $\sigma(T)$. This approach is useful for cylinder specimens, in which the estimation of the radius and/or volume is difficult. An experiment in which aluminum underwent accumulative roll bonding, which is a severe plastic deformation process, validated this method of evaluating σ as a function of the fraction of high-angle grain boundaries. *Published by AIP Publishing.* [http://dx.doi.org/10.1063/1.4950868]

I. INTRODUCTION

The standard approach to measuring electrical conductivity is the so-called four-terminal method, in which two terminals for current and two terminals for voltage are prepared. In studies of the electrical properties of samples with a characteristic size on the micrometer scale, this approach requires special techniques to prepare four terminals on the micrometer samples. In particular, it is very difficult to construct the setup for measuring the electrical conductivity of nanocrystals, nanotubes, or both. The contactless electrical conductivity measurement is useful for examining the above case.

Contactless electrical conductivity measurements generally use (1) the induction current (e.g., eddy current),[1–5] (2) a torque,[6] (3) a force (the Lorentz force,[7] dielectric force,[8] or atomic force[9–11]), (4) reflected electromagnetic waves,[12–14] or (5) resonance.[15] These methods are applied to macroscopic measurements, such as the evaluation of an entire bulky sample,[12–14] and microscopy, such as tomography[16] or imaging of nanomaterials (e.g., nanoparticles[8–11], nanowires,[17] and biological tissues[18–20]). Macroscopic methods have been applied, for example, to the study of nonferromagnetic metals with unique shapes,[5] liquid metals,[6] aerodynamically levitated melts,[21] nanoparticles,[15] and semiconductors.[12–14] In semiconductors, an AC field at a high frequency (up to the gigahertz level) is applied to the target material.[12–14] However, this contactless approach has not been used for electrical study of condensed matter at temperatures from liquid helium temperature to room temperature.[21] This method does not require the preparation of electrical terminals on the target material, so it offers many benefits for the study of condensed matter physics.

Below we review the contactless electrical conductivity measurement using the eddy current via the AC susceptibility of a cylinder sample. In SI units, a dimensionless frequency θ^2 is defined as

$$\theta^2 = 2\pi f \mu_0 \sigma a^2, \tag{1}$$

where f is the frequency of the AC magnetic field H_{AC} = $h \sin 2\pi f t$ (where h is the AC field amplitude, and t is time), μ_0 is the permeability of free space, σ is the electrical conductivity, and a is the radius of the cylinder specimen.[22] Eq. (1) means that if a and the volume V of a specimen can be estimated, we can evaluate σ from the AC susceptibility in the SI units. In the low frequency limit ($\theta \to 0$), σ of the nonmagnetic infinite cylinder is changed via the out-of-phase AC susceptibility (χ'') as $\chi'' = \theta^2/8$.[1,3] The deviation of σ via χ'' is applicable to weakly magnetic conducting disks.[3] Next this approach is expanded to conducting disks with finite aspect ratios ($\gamma = l/a$, here $2l$ is the thickness of the cylinder)[23] via the finite-element method, with the help of numerical studies of the magnetometric demagnetizing factors.[24,25] Additionally, in 2010, Chen and Skumryev measured σ over the wide f range and wide temperature (T) range, as described in detail in Sec. II, and its approach was used to calibrate the eddy current effect due to metallic parts of the equipment itself around the detection coils in the AC magnetic susceptibility measurement system.[22]

Herein, we apply the above approach for the contactless measurement of the relative electrical conductivity σ_n at temperatures over the wide temperature range for the specimens, in which it is difficult to evaluate a and V. In this method, the eddy current is generated under an AC magnetic field.[4,22]

a)Electronic address: mitoh@mns.kyutech.ac.jp

As the frequency of the AC magnetic field increases, the eddy current increases. The skin depth is, however, inversely proportional to the square root of the frequency, so that at high frequencies, the skin effect must be considered.[23] Thus, a low frequency is desirable for conventional evaluation. This contactless measurement of $\sigma_n(T)$ would be applicable to the study of nanocrystalline metals, complex materials with microsize grains, liquid metals, and so on.

Now, this contactless approach of $\sigma_n(T)$ is used for industrial materials, in which it is difficult to evaluate the volume precisely and the skin effect cannot be ignored perfectly. With the help of the four-terminal method at room temperature, the data of $\sigma_n(T)$ can be transformed into those of $\sigma(T)$. The above combined approach is useful for the comparison of $\sigma(T)$ over some industrial materials, because the measurement error of V does not influence the evaluation of σ.

Severe plastic deformation (SPD) processes such as accumulative roll bonding (ARB) [Fig. 1(c), inset][26,27] and high-pressure torsion[28,29] are an effective approach to deformation of the microstructure of a material with an accompanying decrease in the grain size. The ARB process is described in detail later. In this process, the density of grain boundaries increases as the grain size decreases. The grain boundaries strongly affect the mechanical strength. The microsize grains, mechanically created using SPD, are considered to be randomly linked to each other at grain boundaries. For a material with many grain boundaries, when considering a simple path of electrical conductivity, the four-terminal method detects the summation of (1) the electrical resistance within each grain and (2) the concentrated resistance due to the point contacts bridging many grains, which are located between electrical contacts [see Fig. S1(a) of the supplementary material].[30] The influences of vacancies and dislocations are also assumed to be present.[31] Indeed, we experimentally observe these parallel connections. In single pure metals such as Al, Cu, Ag, and Au, conventional electrical conductivity measurement to investigate the influence of the plasticity requires a long specimen with a small cross section because of the high electrical conductivity of these materials. For instance, in a study of a commercial-purity aluminum with a purity of 99.1 wt.% (two-nine),[31,32] denoted as 2N-Al, the prepared size was about 1 mm × 1 mm × 180 mm.[31,33] Indeed, in low-temperature measurements of the electrical conductivity, the effect of plasticity is easily observed because lattice vibration has less effect. In this setting, however, it is difficult to cool a long specimen to the liquid helium temperature and stabilize the sample temperature at an arbitrary value. On the other hand, contactless electrical conductivity using eddy currents can be used to detect the summation of (1) the electrical conductivity within each grain and (2) that via several grains, which are located between electrical contacts [see Fig. S1(b) of the supplementary material].[30] When the grains are linked weakly, the former becomes the main contribution. Indeed, in the specimens with grains strongly linked each other, the data observed in this contactless approach should be consistent with those in the four-terminal method.

The eddy current increases with increasing AC magnetic field according to the Faraday law. The contactless approach of $\sigma_n(T)$ using the eddy current is promising for metallic materials, in which the evaluation of the volume is difficult. Further, investigations of the strain release just after SPD hesitate the time-consuming preparation of electrical contacts. Furthermore, the contactless procedure enables us to use the same sample in studies of the effects of annealing so that there is no sample dependence in a series of annealing experiments.

In this paper, we describe the method of contactless electrical conductivity measurement of $\sigma_n(T)$ for the industrial materials and transform $\sigma_n(T)$ into $\sigma(T)$ by referring to σ at room temperature, obtained by the four-terminal method. Finally, we illustrate the benefits of the above method by presenting a successful study on the correlation between the electrical conductivity and the microstructures in 2N-Al experiencing the SPD process.
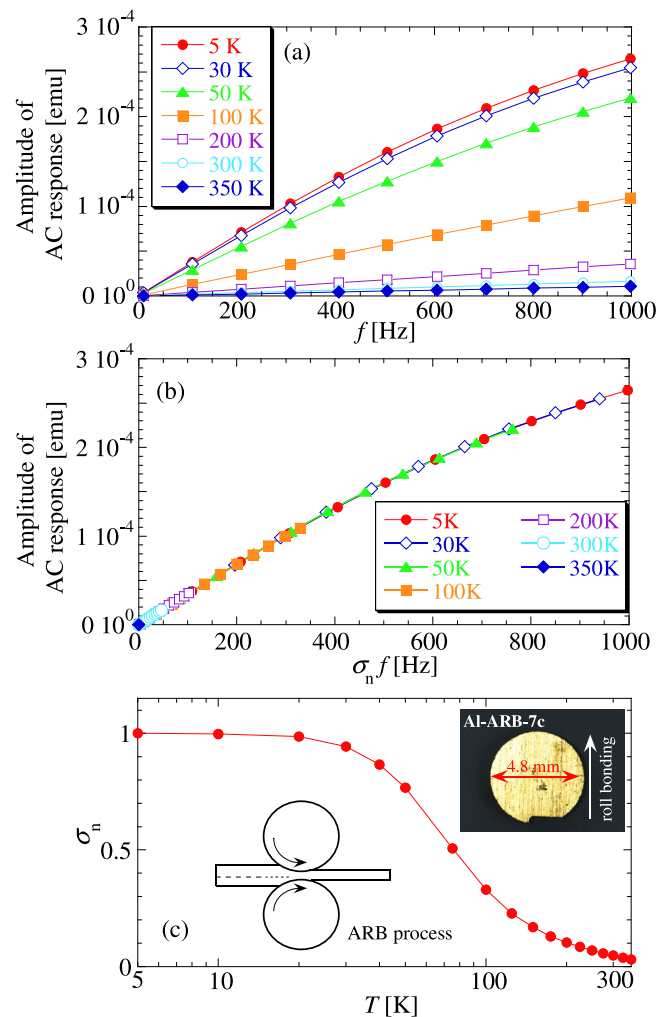

FIG. 1. Analytic flow of contactless electrical conductivity measurement using a magnetometer. (a) Amplitude of the AC magnetic response (A) as a function of frequency f in aluminum after the accumulative roll bonding (ARB) process with a cycle number N_c of 10. (b) Normalized AC response obtained by multiplying f by a normalization factor proportional to the electrical conductivity (σ_n). (c) Electrical conductivity normalized by that at 5 K as a function of T. Insets show the Al-ARB-7c sample and the ARB process. Sample diameter is approximately 4.8 mm, so it is a suitable size for insertion into a commercial SQUID magnetometer. Each specimen has a mark to indicate the direction of roll bonding, as seen in the inset of (c).

II. CONTACTLESS ELECTRICAL CONDUCTIVITY MEASUREMENTS

As mentioned above, Chen and Skumryev investigated the eddy-current demagnetizing effects to evaluate σ for wide f- and T- ranges: Both the amplitude of the AC magnetic susceptibility and its phase delay versus the AC field are normalized with respect to a dimensionless frequency θ^2 related to both the frequency of the AC field (f) and the measurement temperature (T) as shown in Eq. (1).[22] On the right-hand side of Eq. (1), the physical quantity as a function of T is the electrical conductivity σ. When the electrical conductivity of a targeted material with a constant a is studied as a function of T, the AC magnetic magnetization $M = A \sin(2\pi f t - \phi)$ is measured at a fixed T as a function of f. Here, A is the amplitude of AC magnetic response, and ϕ is the phase delay against the AC field.

In the present study, we measured the magnetization M under an AC magnetic field $h \sin(2\pi f t)$ by a commercial superconducting quantum interference device (SQUID) magnetometer. Figure 1 shows the flow of the experimental procedure using the data for 2N-Al experiencing SPD ($\gamma \sim 0.22$). Specimen preparation is described in the next paragraph. Figure 1(a) shows the f dependence of the amplitude of the AC magnetic response (i.e., the AC magnetization) M. The volume of specimens used in this study was on the order of 20 mm^3; each specimen had a mark to indicate the direction of roll bonding [see the inset of Fig. 1(c)]. In practice, it is difficult to evaluate the volume at an accuracy on the order of 0.1 mm^3. Therefore, we prefer the CGS unit to the SI unit as the unit of A, so that we cannot estimate the absolute value of σ from A. First, we notice that monotonous increases in both A [Fig. 1(a)] and $|\phi|$ are measured with increasing f. According to Chen and Skumryev, both A and ϕ must be normalized using f multiplied by σ. For instance, in Fig. 1(b), all data of A are normalized by the data at the minimum temperature in these measurements, $T = 5$ K, so the normalization factor with respect to the horizontal axis is the relative electrical conductivity σ_n against that at $T = 5$ K. Here, σ_n is a function of T. As for ϕ, the normalization procedure to evaluate σ_n, especially at high f, is confused by the eddy current effects intrinsic to the equipment. The analytic results on A are more confident than those on ϕ. Thus, we obtain the temperature dependence of σ_n, as shown in Fig. 1(c). In the analysis of Fig. 1(b), there is only one fitting parameter that is σ_n. This evaluation method of σ_n is valid in emu units as well as SI units.

Commercial 2N-Al sheets underwent SPD by the ARB process.[26,27] The initial sheets of commercial 2N-Al were annealed at 400 °C for 30 min, and the mean grain size was 24 μm. ARB was performed at room temperature using a two-high rolling mill, and the surfaces of the rolls were lubricated by machine oil to reduce the friction of the surface. The ARB process repeats the procedures of cutting a sheet in two, applying a surface treatment, stacking the two sheets, and roll bonding; the huge plastic strain produces ultrafine grains that are smaller than 1 μm.[26,27] A specimen processed by ARB for N cycles is denoted as an ARB Nc specimen. In this paper, we also present information on the microstructures of the ARB-processed specimens observed by electron back-scattering diffraction in a scanning electron microscope with a field emission gun. We focus on the fraction of high-angle grain boundaries (HAGBs), f_{HAGBs}, and the mean separation of HAGBs is considered to be equal to the conventional grain size, D, both of which were evaluated using grain boundary maps. Here, HAGBs are boundaries having misorientation angles larger than 15°. Before the present experiment, we successfully evaluated the electrical conductivity of silver microcrystals (325 mesh, average size of 4 μm), whose total mass was approximately 370 mg. We found that if the target material is a good electrical conductor without magnetic impurities, this contactless electrical conductivity measurement does not require a specimen with large volume. In this paper, the method will be validated by electrical conductivity measurements of 2N-Al after SPD. Four measurement specimens, Al-ARB 7c–10c, were prepared by electric discharge processing, as shown in the inset of Fig. 1(c), so that their diameter and thickness were about $2a = 4.81 \pm 0.01$ mm and $2l = 1.08 \pm 0.08$ mm, respectively: The aspect ratio γ was approximately 0.22. At room temperature, the skin depth of Al at $f = 1$ kHz is approximately 2.5 mm. There an AC field of $h = 4.0$ Oe with a frequency of up to 1 kHz penetrates the specimens. However, at liquid helium temperature, σ increases up to approximately twenty times as large as that at room temperature, so that the skin depth decreases down to less than 1.0 mm. When σ further increases by annealing, the frequency range must be reduced to the level of 0.5 kHz. The masses of these specimens were 48.9, 52.2, 54.1, and 54.8 mg, respectively. The AC magnetic field was applied in the thickness direction. As N increases from 7c to 10c, D is almost unchanged, whereas f_{HAGBs} continues to increase slightly.[31] In the process, the dislocation density is also almost unchanged, and the density of grain boundaries increases, resulting in an increase in the electrical resistance at $T = 77$ K.[31] Further, each specimen was annealed for 30 min in an air atmosphere at a temperature T_{ann} of up to 400 °C. We represent T_{ann} using the unit of degree Celsius for the sake of simple mathematical expressions, whereas the temperature used in the electrical conductivity measurements is expressed in kelvins.

III. MEASUREMENTS FOR AL-ARB

The specimens used in the present measurements were disks with $\gamma \sim 0.22$. Prior to presenting the data of electrical resistivity $\rho(T)$ and conductivity $\sigma(T)$ as a function of T, we consider the influence of the demagnetizing field. The demagnetizing factor (N_d) depends on both the value of γ and the magnitude of susceptibility. Based on the data of Fig. 1(b) and the table of N_d values in the literature,[25] N_d can vary over the range of 0.60–0.64. However, the demagnetizing field $N_d A$ is a few percent of h at most. Indeed, analysis of the demagnetizing field has little influence on the estimation of σ_n. The effect of skin depth rather than the demagnetizing field may influence the observed value of A. In this study, the demagnetizing field is ignored in the series of analyses. The electrical resistivity measurements by Miyajima *et al.* showed that $\rho(T = 300$ K) does not depend on the cycle number of the ARB process for $N_c = 7$–10 cycles and that its value remains approximately 32 nΩm.[31] Now this value becomes the standard value, so
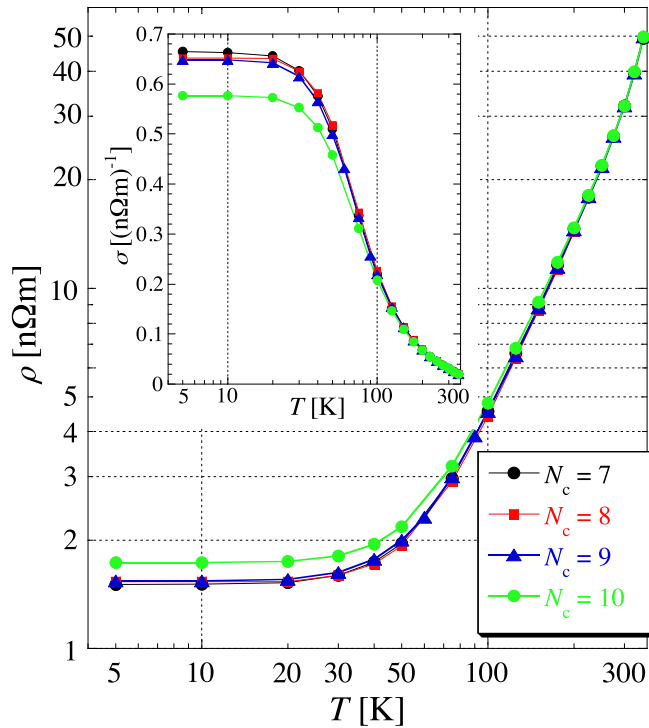
FIG. 2. Temperature dependence of electrical resistivity ρ for Al-ARB 7c–10c ($N_c = 7$–10 cycles). Both horizontal and vertical axes use a logarithmic scale. In the inset, the temperature dependence of electrical conductivity $\sigma (=1/\rho)$ is presented using the horizontal axis with a logarithmic scale. It is known that the electrical resistivity at $T = 300$ K does not depend on N_c, which has a value of approximately 32 nΩm.[31]

that the values of $\sigma_n(T = 300$ K) for $N_c = 7$–10 cycles are transformed into $\sigma = (32$ nΩm$)^{-1}$.

Figure 2 shows the T dependence of $\rho(=1/\sigma)$ and σ for non-annealed Al-ARB 7c–10c ($N_c = 7$–10 cycles) in both linear and logarithmic T-scales. For reference, the data of $\rho(T)$ using two linear scales are prepared, as shown in Fig. S2 in the supplementary material.[30] At $T \geq 300$ K, $\rho(T)$ does not depend on N_c. At $T = 80$ K, there is an increase in ρ of 0.2 nΩm

for the change in $N_c = 7 \rightarrow 10$; this result is quantitatively consistent with the results at $T = 77$ K by Miyajima *et al.*[31] As T decreases, the effect of SPD becomes significant. Figure 2 shows that σ, rather than ρ, is suitable for evaluating the SPD effect. When we carefully consider the T region of residual resistance, the decrease in σ is remarkable as N_c changes from 9 to 10.

Figure 3 shows the effects of annealing on σ for Al-ARB 7c–10c. For instance, at $N_c = 7$ cycles, as the annealing temperature (T_{ann}) increases, $\sigma(T = 5$ K) increases, whereas it turns to decrease at a T_{ann} of approximately 230 °C. The magnitude of $\sigma(T = 5$ K) at $T_{ann} = 400$ °C is located between that at $T_{ann} = 180$ °C and at $T_{ann} = 200$ °C. This annealing effect was also observed at the other annealing temperatures. For all values of N_c, $\sigma(T)$ has a maximum at approximately 230 °C, and, interestingly, the magnitude is almost independent of N_c.

The phenomenon described above is clearly illustrated in Fig. 4, which shows the T_{ann} dependence of $\rho(T = 5$ and 75 K) for Al-ARB 7c–10c. All of the Al-ARB materials exhibit a similar T_{ann} dependence. For T_{ann} of up to 230 °C, Al-ARB 10c exhibits the largest difference between $\rho(T = 5$ K) before annealing (RT) and after annealing at $T_{ann} = 230$ °C. Here, $\rho(T = 75$ K) also behaves similarly to $\rho(T = 5$ K). The electrical resistance for a T_{ann} of up to 250 °C has already been measured at 77 K by the contact four-probe method, and the results obtained there are consistent with the present data.[33]

Figure 5 shows the effects of annealing on the metallographic structure represented by the grain size (D) and HAGB density (f_{HAGB}) for Al-ARB with $N_c = 10$ cycles, presented by Terada (one of the authors) *et al.*[34] As T_{ann} increases, D continues to increase, whereas f_{HAGB} has a minimum at approximately 230 °C. The above change in D is consistent with the data in a previous study.[33] If the increase in D was an intrinsic factor in the change in σ_n, then σ_n would increase with increasing T_{ann}. This scenario is, however, inconsistent with the experimental facts. The initial decrease in f_{HAGB} shows that the metallographic structure tends to be uniform,
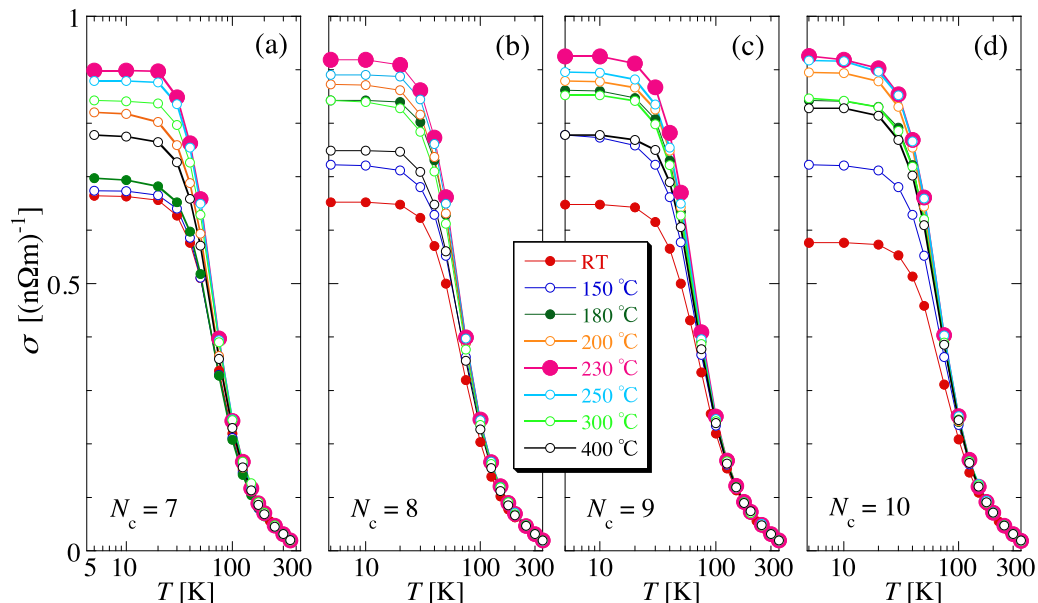

FIG. 3. Temperature dependence of electrical conductivity σ for annealed Al-ARB 7c–10c ($N_c = 7$–10 cycles) at the annealing temperature (T_{ann}). RT means room temperature.
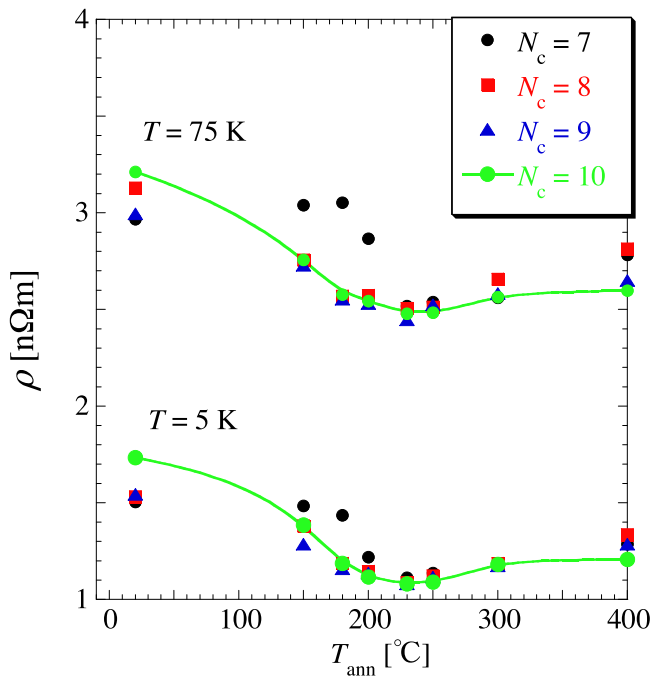
FIG. 4. Annealing temperature (T_{ann}) dependence of electrical resistivity ρ at $T = 5$ K and 75 K for annealed Al-ARB 7c–10c ($N_c = 7$–10 cycles). Solid curves for Al-ARB 10c are guides for the eyes.

suggesting a reduction in electronic scattering at the grain boundary. The dislocation density also has a minimum at approximately 200 °C.[33] Indeed, these behaviors of the structural misorientation are physically consistent with the increase in σ (and the decrease in ρ). The T_{ann} values at the minimum
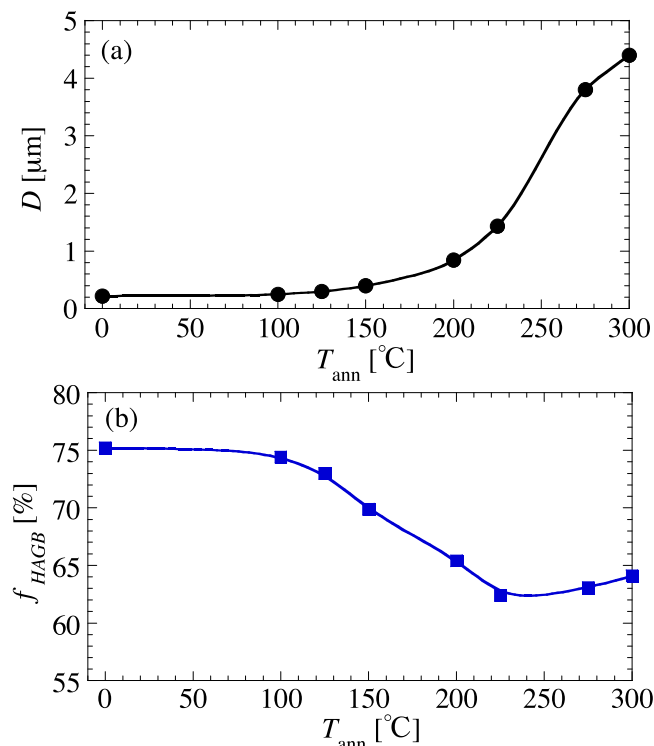

FIG. 5. Annealing temperature (T_{ann}) dependence of (a) the grain size (D) and (b) the fraction of the high-angle grain boundaries (HAGBs) f_{HAGB} for Al-ARB 10c.

f_{HAGB} and minimum dislocation density are consistent with that at the maximum σ (i.e., the minimum ρ), as seen in Fig. 4. Thus, σ reflects the degree of structural misorientation rather than the grain size. For reference, the starting sheets prior to the ARB process were annealed at 400 °C, which was sufficiently high for Al. Hereafter, its metallographic structure does not significantly change for additional annealing below 400 °C.

To quantitatively investigate the effects of annealing on the electrical conductivity, it is desirable to continue to use the same sample over a series of measurements. If the contact method is adopted, the electrode is oxidized in the process of annealing, and the measurement reliability may be reduced. The present contactless method easily eliminates this disadvantage. We have successfully measured the electrical conductivity of assembled silver nanopowders, each of which has a size of approximately 3 nm (see Figs. S3 and S4[30] of the supplementary material), as well as silver micropowders with a size of approximately 4 μm (see Fig. S5[30] of the supplementary material). The present contactless method is applicable to a nonferromagnetic metal with a wide range of volumes. It has the advantage of providing easy evaluation of the structural strain using a conventional magnetic measurement.

ACKNOWLEDGMENTS

[1]R. M. Mozorth, *Ferromagnetism* (D. Van Nostrand Company, Inc., New York, 1951).
[2]Y. Kraftmakher, Meas. Sci. Technol. **2**, 253 (1991).
[3]D.-X. Chen and A. Hernando, J. Appl. Phys. **73**, 6852 (1993).
[4]M. Miletić, P. M. Nikolić, D. Vasiljević-Radovic, and A. I. Bojičic, Rev. Sci. Instrum. **68**, 3523 (1997).
[5]J. Iniguez and V. Raposo, Eur. J. Phys. **28**, 1125 (2007).
[6]S. Bakhtiyarov and R. Overfelt, J. Mater. Sci. **34**, 945 (1999).
[7]R. P. Uhlig, M. Zec, M. Ziolkowski, H. Brauer, and A. Thess, J. Appl. Phys. **111**, 094914 (2012).
[8]W. Lu, J. Zhang, Y. Li, Q. Chen, X. Wang, A. Hassanien, and L. Chen, J. Phys. Chem. C **116**, 7158 (2012).
[9]L. Zhang, Y. Ju, A. Hosoi, and A. Fujimoto, Rev. Sci. Instrum. **81**, 123708 (2010).
[10]L. Zhang, Y. Ju, A. Hosoi, and A. Fujimoto, Appl. Phys. Express **5**, 016602 (2012).
[11]C. Prastani, A. Vetushka, A. Fejfar, M. Nanu, D. Nanu, J. Rath, and R. Schropp, Appl. Phys. Lett. **101**, 083107 (2012).
[12]Y. Ju, K. Inoue, M. Saka, and H. Abe, Appl. Phys. Lett. **81**, 3585 (2002).
[13]Y. Ju, Y. Ohno, H. Soyama, and M. Saka, J. Mater. Sci. Technol. **20**(Suppl. 1), 123 (2004).
[14]Y. Ju, Y. Hirosawa, H. Soyama, and M. Saka, Appl. Phys. Lett. **87**, 162102 (2005).
[15]K. Padmalekha and S. V. Bhat, Solid State Commun. **150**, 1518 (2010).
[16]B. Wang, Y. Hu, H. Ji, Z. Huang, and H. Li, IEEE Trans. Instrum. Meas. **62**, 1017 (2013).
[17]C. Akin, J. Yi, L. Feldman, C. Durand, S. Hus, A. Li, M. Filer, and J. Shan, ACS Nano **9**, 5405 (2015).
[18]N. Gencer and M. Tek, Phys. Med. Biol. **44**, 927 (1999).
[19]N. Gencer and M. Tek, IEEE Trans. Med. Imaging **18**, 617 (1999).
[20]B. Karbeyaz and N. Gencer, J. Trans. Med. Imaging **22**, 627 (2003).
[21]L. Skinner and A. Barnes, Rev. Sci. Instrum. **77**, 123904 (2006).
[22]D.-X. Chen and V. Skumryev, Rev. Sci. Instrum. **81**, 025104 (2010).
[23]D.-X. Chen and C. Gu, IEEE Trans. Mag. **41**, 2436 (2005).
[24]R. B. Goldfarb and J. V. Minervini, Rev. Sci. Instrum. **55**, 761 (1984).
[25]D.-X. Chen, J. A. Brug, and R. B. Goldfarb, IEEE Trans. Mag. **27**, 3601 (1991).

[26]A. Azushima, R. Kopp, A. Korhonen, D. Yang, F. Micari, G. Lahoti, P. Groche, J. Yanagimoto, N. Tsuji, A. Rosochowski *et al.*, CIRP Ann. Manuf. Technol. **57**, 716 (2008).

[27]Y. Saito, H. Utsunomiya, N. Tsuji, and T. Sakai, Acta Mater. **47**, 579 (1999).

[28]N. A. Smirnova, V. I. Levit, V. I. Pilyugin, R. I. Kuznetsov, L. S. Davydova, and V. A. Sazonova, Fiz. Met. Metalloved. **61**, 1170 (1986).

[29]Y. Harai, Y. Ito, and Z. Horita, Scr. Mater. **58**, 469 (2008).

[30]See supplementary material at http://dx.doi.org/10.1063/1.4950868 for overview of contactless electrical conductivity, electrical resistivity for Al-ARB 7c-10c, TEM picture and electrical resistivity of diffused Ag nanoparticles, and electrical resistivity of Ag microparticles.

[31]Y. Miyajima, S. Komatsu, M. Mitsuhara, S. Hata, H. Nakashima, and N. Tsuji, Philos. Mag. **90**, 4475 (2010).

[32]Y. Miyajima, M. Mitsuhara, S. Hata, H. Nakashima, and N. Tsuji, Mater. Sci. Eng. A **528**, 776 (2010).

[33]Y. Miyajima, S. Komatsu, M. Mitsuhara, S. Hata, H. Nakashima, and N. Tsuji, Philos. Mag. **95**, 1139 (2015).

[34]D. Terada, H. Takarada, and N. Tsuji, private communication (2015).